ACS APPLIED NANO MATERIALS

www.acsanm.org Article

Ultradense Arrays of Sub-100 nm Co/CoO Nanodisks for Spintronics Applications

R. Morales, A. N. Flores, Nicolas M. Vargas, J. Giuliani, Ivan K. Schuller, and C. Monton*

Cite This: https://dx.doi.org/10.1021/acsanm.0c00052 Read Online

ACCESS | Metrics & More | Article Recommendations

ABSTRACT: Sub-100 nm ferromagnetic/antiferromagnetic nanodisks present enhanced magnetic properties with respect to their thin film counterparts. Co/CoO disks were fabricated over large areas by a transferring process of an anodic aluminum oxide membrane, electron beam evaporation of Co, and subsequent oxidation to CoO. This method reveals exchange bias fields up to 4 times larger than that in thin films and higher blocking temperatures for the same oxidation protocol. The significant improvement of the magnetic properties is attributed to finite-size effects in nanostructures and might be exploited in diverse areas such as the magnetic stabilization of ultradense arrays or the scalability process of patterned heterostructures in spintronic phenomena.

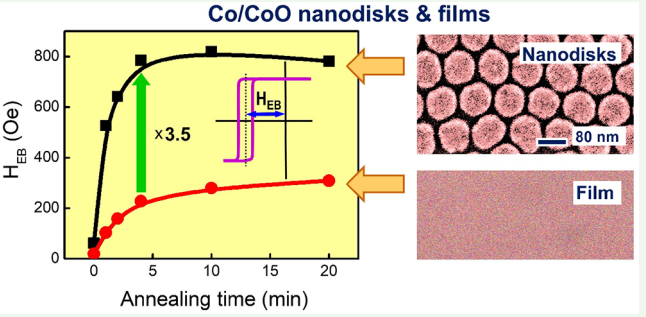

KEYWORDS: *exchange bias, magnetic nanostructures, anodic aluminum oxide, exchange interactions, blocking temperature*

INTRODUCTION

The scalability of the physical properties of materials is commonly used to improve or develop new technological applications. Performance of magnetic-based devices may change when reducing the size of magnetic elements.[1−3] For instance, materials exhibiting perpendicular magnetic anisotropy in thin films cannot preserve this property below a critical size,[4] or vice versa, reorientation from in-plane to out-of-plane magnetization might occur upon shrinking the lateral dimension of the sample.[5] A critical case is the superparamagnetic limit at which the material loses long-range order (i.e., ferromagnetism) with the consequent loss of technological interest.[6] Conversely, size changes can lead to new and appealing properties as the material dimensions compare to magnetic length scales. Vortex state and onion spin configurations are only possible in nanodisks and nanorings with specific dimensions.[7,8] Nanomagnets with unique spin configurations have recently attracted much attention for their high capabilities in storage media, logic and communication applications, and novel biomedical practices.[9−14]

Exchange bias (EB) is an important ingredient in the design of magnetic sensors, nonvolatile memories, and electronic and spintronic devices.[15−17] It takes place at the interface between ferromagnetic (FM) and antiferromagnetic (AFM) materials and is characterized by a shift of the magnetization curve along the field axis.[18] Other phenomena such as an increase of the coercive field, asymmetric hysteresis loops, and training effects are distinctive features of the EB and strongly dependent on the properties of the FM and AFM.[19−21] The structure of the FM/AFM interface, roughness, chemical inhomogeneity, grain boundaries, and crystallographic order determine the strength of the exchange bias field (H_{EB}) and the blocking temperature (T_B), above which the exchange bias disappears.[22−28]

The EB phenomenon is also affected by scaling effects. Studies in thin films demonstrated the dependence of EB on the FM and AFM thickness[29−32] and a minimum AFM thickness for the onset of EB.[33,34] Lateral confinement can strongly influence the properties of magnetic nanostructures.[12,35−37] The low coordination of AFM spins at the surface, and a small AFM volume in nanostructures produces a drop of the T_B and a reduction of the H_{EB} as compared to the FM/AFM thin film.[38−40] Although some authors claimed enhancement of the H_{EB} in magnetic nanostructures,[41,42] improvement of both magnetic parameters, T_B and H_{EB}, has not been reported in FM/AFM nanostructures.

In this article, we show enhanced thermal stability (T_B) and larger exchange bias fields (H_{EB}) of sub-100 nm Co/CoO nanodisks compared to continuous thin films. The nanopatterning process significantly improves the magnitude of the

Received: January 7, 2020
Accepted: April 16, 2020
Published: April 16, 2020

https://dx.doi.org/10.1021/acsanm.0c00052
ACS Appl. Nano Mater. XXXX, XXX, XXX−XXX

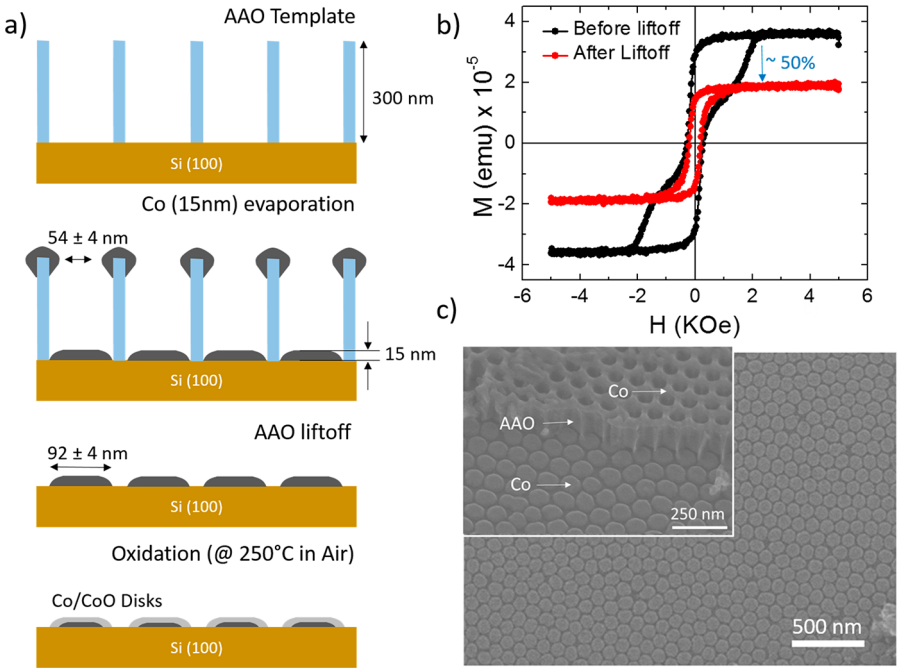

Figure 1. (a) Fabrication process of the Co nanodisks. (b) Hysteresis magnetization loops of the sample before and after the liftoff process. The 50% reduction in the saturation magnetization accounts for the Co on top of the AAO membrane, which is removed during liftoff. (c) Nanodisks after liftoff. This image is representative of the total (3 mm × 25 mm) area of the sample. In the inset, the AAO was partially removed to show the fabrication process.

exchange bias field by a factor of up to 4 and increases by 25% the blocking temperature of the Co/CoO system. Moreover, this enhancement was achieved in ultradense arrays of disks (Tb/in.^{2}). These findings have a positive impact on the stabilization of Co nanomagnets and their use in spintronic designs, as lateral giant magneto-resistance,[43] current-induced spin−orbit torque,[44] tunneling anisotropic magneto-resistance with CoO barrier,[45] or magneto-ionic devices.[46]

Cobalt is a FM widely used in magnetic recording media, and CoO is an AFM which exhibits high magneto-crystalline anisotropy and a moderate Néel temperature (T_N = 290 K).[15,47−52] In the case of Co nanostructures, the formation of a few nanometer thick CoO layer on the surface due to oxygen exposure promotes the appearance of an EB field (H_{EB}) that significantly modifies the magnetic behavior of the system. For this reason, Co/CoO nanostructures have been a subject of intense research.[16,40,53−57]

EB nanostructures are typically fabricated by using lithographic techniques. However, there has been a strong interest in the development of alternative fabrication routes to fulfill the continued scalability of spintronic devices and the need for increasing their magnetic recording density. Anodic aluminum oxide (AAO) nanoporous templates have emerged as a strong contender among several nonlithographic techniques because it overcomes the costs, minimum size, and area limitations of photo and electron beam lithography techniques.

■ FABRICATION AND CHARACTERIZATION

Ultradense (Tb/in.^{2}) arrays of Co nanodisks were grown onto a Si (100) substrate by using anodic aluminum oxide (AAO) membranes as a shadow mask (Figure 1a). The AAO masks (300 nm thick, 92 nm pore diameter) were transferred onto the substrate following the procedure described in ref 58. A 15 nm thick Co layer was deposited on the Si/AAO substrate by electron beam evaporation in a high-vacuum chamber with a base pressure of 10^{-7} Torr. Continuous thin films were simultaneously deposited on Si (100) wafers for comparison. After codeposition, the AAO membrane was removed by using low power sonication for 30 min by submerging the sample in a beaker with methanol. The successful liftoff of the membrane was verified by scanning electron microscopy (SEM) and magnetic measurements. Figure 1b shows the hysteresis magnetization loops of the sample before and after liftoff. The observed 50% reduction in the saturation moment after liftoff corresponds to the amount of Co deposited on top of the AAO. This perforated Co film was removed during liftoff, and its amount correlates with the porosity of the AAO membrane[59] (i.e., $0.907(D_p/D_c)^2 \times 100 \approx 60\%$, where D_p = 92 nm and D_c = 110 nm are the pore diameter and center-to-center inter pore distance, respectively). The final hysteresis loop (red) is also consistent with the total removal of the perforated Co film that exhibits a large coercivity in the initial curve (black).

Figure 1c shows the SEM image of the array of Co nanodisks after liftoff. Microscopy image segmentation analysis (MIST)[60] of SEM images shows that the disks are monodisperse with a mean diameter of 92 ± 5 nm and a center-to-center distance of 110 ± 7 nm. In the inset of Figure 1c, we performed a partial removal of the AAO template to illustrate the sample fabrication process.

Figure 2 compares the hysteresis loops of disks and film of "as grown" and annealed samples. All the hysteresis loops were measured up to H_{max} = 10 kOe to saturate the sample. To ensure reproducibility, film and disks samples were annealed side-by-side at 250 °C in air, in incremental times as follows: 1 min, + 1 min (accumulated 2 min), + 2 min (accumulated 4 min), + 6 min (accumulated 10 min), and +10 min (accumulated 20 min). After each annealing, the magnetization curves were measured in the whole temperature range.

https://dx.doi.org/10.1021/acsanm.0c00052
ACS Appl. Nano Mater. XXXX, XXX, XXX−XXX

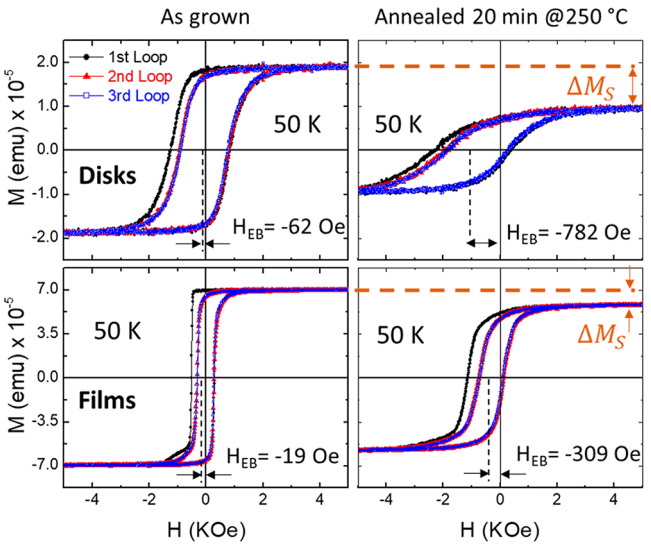

Figure 2. Exchange bias and training effect in disks (upper panels) and reference film (lower panels) at 50 K of "as grown" and annealed samples. No magnetic field was applied during annealing, but the Co was magnetically oriented at remanence. The H_{EB} values in each panel correspond to the third loop. ΔM_S represents the change of the magnetic moment after annealing, and it is used to determine the reduction of the Co thickness.

Magnetic hysteresis loops were performed in a vibrating sample magnetometer (VSM) with the applied field parallel to the substrate. In all the cases, measurements started at 50 K after cooling the samples in the remnant state after a previous saturation at 3 T. Because the normalized remanence of disks and films is close to 1, similar results were observed when the samples were cooled with a 3 T applied field.

Two main features are observable in Figure 2. On the one hand, the hysteresis loops show a magnetic moment Δm_s reduction in annealed samples. This reduction can be used to estimate the amount of Co remaining in the samples after oxidation. Thus, the CoO layer increases with longer annealing times. Moreover, Co disks oxidize faster than thin films, since Δm_s is more pronounced in the nanodisks hysteresis loops. On the other hand, nanodisks show a higher exchange bias field, $H_{EB} = (H_{c1} + H_{c2})/2$, than the thin film; H_{c1} and H_{c2} are the left and right coercive fields, respectively. Both systems show training effects, but magnetization curves overlap after the third cycle, so the H_{EB} was calculated from the third hysteresis loops.

The temperature dependence of the H_{EB} for the three consecutive hysteresis loops recorded at each temperature is plotted in Figure 3. Starting at 50 K, the temperature was increased in 25 K increments up to 300 K. The blocking temperature of the EB system can be estimated from these data as the temperature at which the H_{EB} vanishes (red arrow). The same temperature and field scales in the four panels reveal a striking training effect in both nanodisks and films, although "as grown" samples did not undergo thermal annealing. This effect is due to a thin native CoO layer that promotes EB below a low blocking temperature (T_B < 85 K). The temperature dependence of training effects in annealed disks and films is very similar and reveals the intrinsic nature of metastable states in the antiferromagnetic CoO.

Both relevant parameters, H_{EB} and T_B, are shaped by the microstructure created during the oxidation process and, consequently, affected by the annealing time as shown in Figure 4. The magnitude of the H_{EB} increases faster in

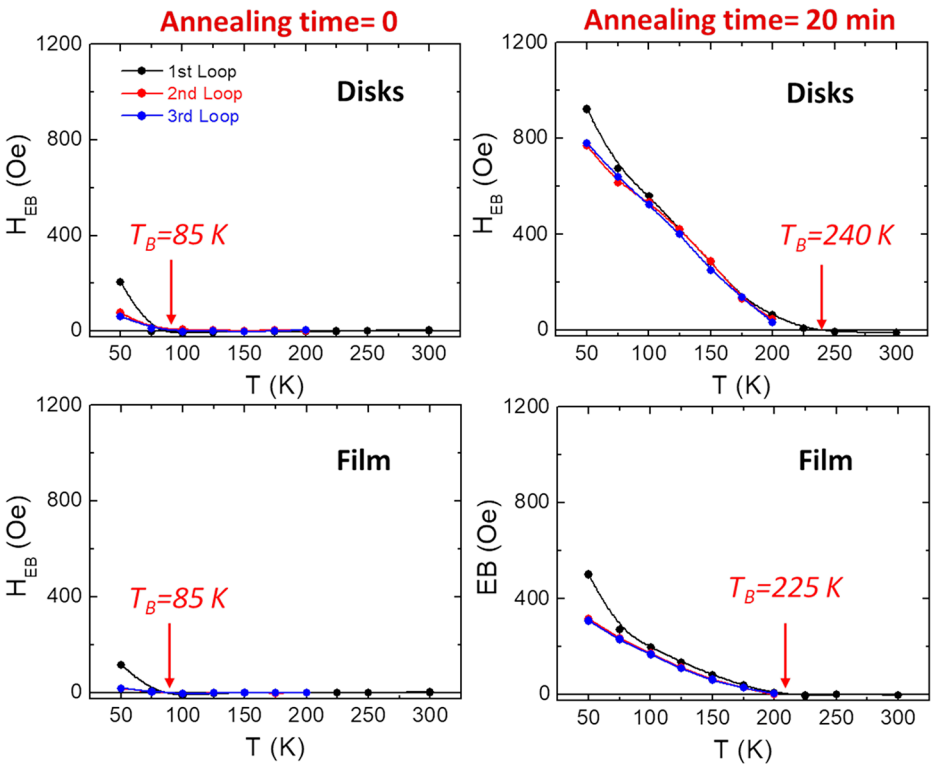

Figure 3. Training effect and blocking temperature as a function of temperature and oxidation time for disks and films. Black, red, and blue circles represent the first, second, and third loop, respectively.

https://dx.doi.org/10.1021/acsanm.0c00052
ACS Appl. Nano Mater. XXXX, XXX, XXX−XXX

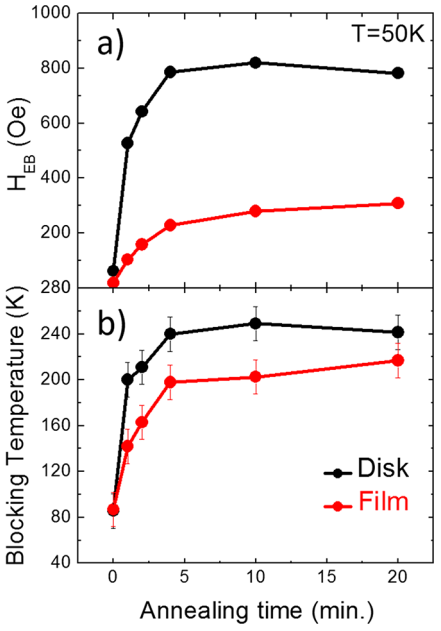

Figure 4. Exchange bias and blocking temperature for disks and films as a function of the oxidation time. The H_{EB} values are obtained from the third loop recorded at each oxidation time.

patterned structures than in thin films (Figure 4a). Nanodisks reach a maximum after 10 min of oxidation, whereas it takes more than 20 min for the film. Most importantly, the magnitude of the H_{EB} at 50 K is almost up to 4 times larger for nanodisks for short annealing times. This is a highlighted finding of the patterning process and scalability feature of the presented Co/CoO system, with an enhancement factor superior to other equivalent nanostructures.[39,40]

The blocking temperature as a function of the oxidation time is plotted in Figure 4b. Interestingly, the nanodisks reach the maximum T_B = 250 °C after only 4 min of oxidation. It takes 20 min for the films to achieve a similar value. The T_B of the nanomagnets is always higher than that of the film for any annealing time. This is a surprising result since the thermal stability of an EB system usually decreases with the volume of the AFM material due to a dimensionality effect on the magnetic anisotropy energy of AFM pinned spins.[2] Previous works on nanostructured EB films present such a reduction.[39,40,61]

DISCUSSION

To account for the significant difference between nanodisks and films and shed light on the intrinsic or structural origin of the enhanced properties of the nanostructures, two geometrical models were investigated (Figure 5a).

Model 1 illustrates a simple approach for a straightforward comparison with thin films. Starting with the ideal disk shape before any oxidation, model 1 assumes that the oxidation only occurs on the top surface of the disk, equivalent to the oxidation process in a thin film. Thus, Figure 5a allows us to calculate the remaining Co thickness after oxidation from the final and initial magnetic moments measured at saturation in Figure 2 ($\Delta m_s = m_s^f - m_s^i$). Hence, the final Co thickness is given by $t_{Co}^f = (m_s^f/m_s^i)t_{Co}^i$. The same formula can be applied to thin films and model 1 nanodisk. However, the measured reduction of m_s is different for films and nanostructures (Figure 2). Consequently, the remaining t_{Co} follows a different dependence with the annealing time (Figure 5b). Δm_s is larger for nanostructures for each oxidation time, and t_{Co} is thinner than the remaining Co layer of thin films.

The thickness of the FM layer is a required parameter to calculate the exchange energy density (σ) at the FM/AFM interface. σ was estimated with the known values of H_{EB} and t_{Co} plotted in Figures 4a and 5b, and the Co metal magnetization, M_{Co} = 1440 emu/cm^3.[15]

$$\sigma = M_{Co} t_{Co} H_{EB} \quad (1)$$

Figure 5c reveals that the exchange energy density is around 2.5 times larger in nanodisks than in films for oxidation times shorter than 5 min. Although this difference tends to decrease with annealing time, the value of σ remains higher in patterned structures. The exchange energy density is an intrinsic magnitude directly related to the density of pinned uncompensated AFM spins at the FM/AFM interface, the crystalline quality of the AFM, and its interface with the FM layer. Thus, it is surprising that following the same annealing process, disks and films present quite different exchange interactions.

To discard a geometrical origin, model 2 considers a more realistic case taking into account lateral oxidation of nanodisks. In this case, the same CoO thickness covers the top surface of the dot and the lateral area with a cylindrical shell surrounding the Co core (see cross section in Figure 5a). The remaining Co thickness was calculated for this geometrical model from the variation of the magnetic moment before and after the annealing (Figure 2). The dependence with the oxidation time

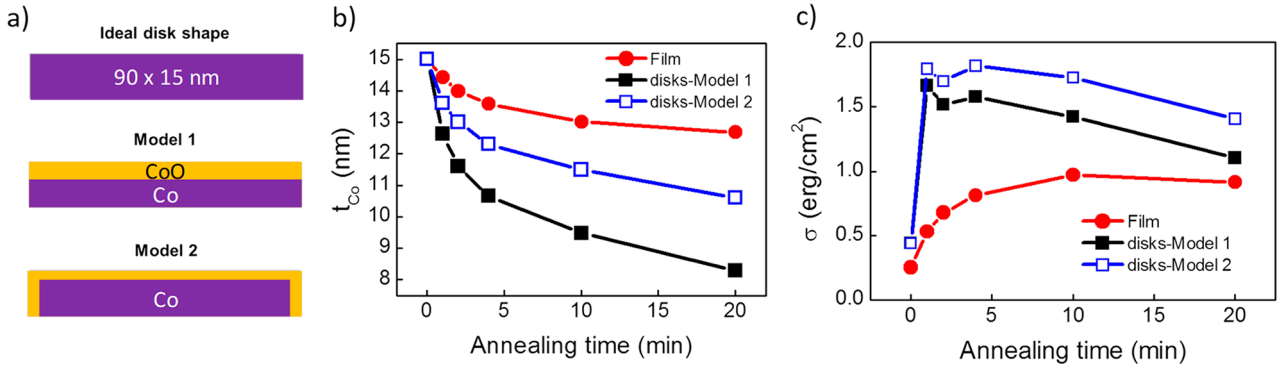

Figure 5. (a) Conceptual description of the Models. (b) Estimated Co thickness reduction upon oxidation (annealing) time obtained by the relative reduction of saturation magnetization (ΔM_S) for different models. (c) Comparative exchange energy density for each geometrical model.

https://dx.doi.org/10.1021/acsanm.0c00052
ACS Appl. Nano Mater. XXXX, XXX, XXX−XXX

is plotted in Figure 5b. Now, the metallic Co layer is thicker than the t_{Co} in model 1. It is an expected result given that the lateral dimension of the Co disk is now smaller, so it must be thicker to preserve the same magnetic moment. The consequence is an increase of the exchange energy density calculated with formula 1 (Figure 5c). Model 2 also points out that to account for the experimental values of EB, the exchange energy density at the Co/CoO interface must be different in core−shell nanodisks and thin films. Thus, the enhancement of the EB phenomenon in Co/CoO nanostructures has an intrinsic origin and is not a structural/geometrical issue. Although such a dense array might be affected by dipolar interaction among dots, there is no clear evidence on the magnetization reversal curves of their effect on the EB field. Dipolar coupling in Co/CoO nanostructures might lead to asymmetrical branches of the hysteresis loop and smaller values of H_{EB}.[55]

The σ plotted for model 2 in Figure 5c was calculated considering the top Co/CoO interface of the dot. No lateral EB effects were taken into account. Although the Co/CoO interface of the shell covers all angles, from 0 to 2π, with respect to the unidirectional anisotropy of the system, it can contribute to the total EB with laterally pinned uncompensated AFM spins. Monte Carlo simulations corroborated this contribution in Au/Co/Au disks with lateral oxidation only.[62] However, reduced values of EB were obtained. Most of the uncompensated spins of the CoO lateral shell reverse with the Co magnetization and do not produce EB, which is dominated by pinned spins at the top CoO surface.[40] Therefore, the lateral mechanism is not enough to account for H_{EB} values 4 times larger in nanodisks than in continuous films.

A plausible scenario that leads to a higher interfacial exchange energy density is a finite-size effect in the AFM material. Malozemoff demonstrated that the interface energy goes inversely with the AFM domain size.[63] Thus, Co/CoO nanodisks with feature size smaller than CoO domains in thin films yield larger exchange energy densities, in agreement with the results in Figure 5c. The dot diameter, 92 nm, is much smaller than the micrometer size domains observed in Co/CoO bilayers by photoemission electron microscopy and the magneto-optical Kerr effect.[64−66] Moreover, intrinsic CoO domains in continuous films can exhibit an averaging effect that is not present in sub-100 nm nanostructures. In this regime, the reversal of FM domains larger than the AFM ones reduces the EB field due to the average of the unidirectional anisotropies experienced by the FM domain.[67−70] The Co/CoO films oxidized in the annealing process at 250 °C present an exchange energy density around 0.97 erg/cm^2 at 50 K, which is similar or even higher than other values in the literature measured at a much lower temperature.[71,72] As a scalability effect, the exchange energy density of nanodisks increases up to 1.80 erg/cm^2 at 50 K, which is also above the magnitude estimated in other equivalent nanostructures. Thus, the simple procedure described in this work provides a validated approach to fabricate high-quality Co/CoO interfaces in both thin films and nanodisks.

It is worth noting that although patterned and nonpatterned samples were simultaneously annealed, both geometrical models estimate thicker CoO layers in nanodisks than in thin films for the same annealing time (Figure 5b). The thickness of the CoO layer determines the blocking temperature of the antiferromagnet. Oxidation times shorter than 2 min create a very thin AFM layer in the continuous film with T_B below 160 K (Figure 4b). However, 1 min oxidation of nanodisks produces a CoO thickness equivalent to 4 min oxidation of the film (model 2 in Figure 5b).

Consequently, both T_B's should be similar for both systems, which is in agreement with the experimental result, T_B = 200 K in Figure 4b. The same equivalence can be established for 2 min oxidation of nanodisks and 20 min in thin films. Thus, there is a correlation between the remaining t_{Co} of films and model 2 (Figure 4b) and the T_B of the two systems (Figure 5b). Annealing times above 4 min generate a CoO layer in nanostructures thick enough to thermally stabilize pinned AFM spins up to 240 K. This T_B remains constant for longer oxidation times. The same trend was observed with EB dependence that saturates upon 4 min annealing (Figure 4a). Therefore, the performance of sub-100 nm Co/CoO nanodisks can be optimized with oxidation times between 4 and 10 min.

CONCLUSIONS

We have successfully used a simple fabrication technique for the synthesis of ultradense Co/CoO sub-100 nm nanodisks with a packaging density of Tb/in.^{2}. This technique uses AAO nanoporous membranes as shadow masks in combination with electron beam deposition of a metallic Co thin film. An antiferromagnetic CoO layer was generated by thermal oxidation in air, and the thickness of the CoO layer was controlled by the oxidation time. The procedure allows us to regulate the magnitude of the exchange bias and the blocking temperature of the system.

Most importantly, nanodisks present a superior performance than Co/CoO thin films, exhibiting stronger EB fields and higher blocking temperatures. Besides, the simple fabrication process yields high exchange energy densities at the Co/CoO interface in both cases, films, and nanodisks. This enhancement is attributed to confinement effects in the antiferromagnet that limit the AFM domain size. To get a deeper insight into the microscopic origin of these results, further studies should be performed using nanometer-scale sensitive techniques. In short, this work takes relevance because it provides a successful fabrication route to synthesize large areas of multifunctional nanostructures with improved magnetic properties. The enhancement of exchange interactions in these nanostructures might be useful in CoO spintronic phenomena, such as giant or tunneling magneto-resistance and magneto-ionic effects.

AUTHOR INFORMATION

Corresponding Author

C. Monton − *Department of Physics and Astronomy, The University of Texas at San Antonio, San Antonio, Texas 78249, United States; General Atomics, San Diego, California 92186, United States;* orcid.org/0000-0003-3472-873X; Email: montonc@fusion.gat.com

Authors

R. Morales − *Department of Physical-Chemistry & BCMaterials, University of the Basque Country UPV/EHU, 48940 Leioa, Spain; IKERBASQUE, Basque Foundation for Science, 48011 Bilbao, Spain;* orcid.org/0000-0003-1733-2039

A. N. Flores − *Department of Physics and Astronomy, The University of Texas at San Antonio, San Antonio, Texas 78249, United States*

https://dx.doi.org/10.1021/acsanm.0c00052
ACS Appl. Nano Mater. XXXX, XXX, XXX−XXX

Nicolas M. Vargas − *Center for Advanced Nanoscience and Department of Physics, University of California, San Diego, La Jolla, California 92093, United States*
J. Giuliani − *Department of Physics and Astronomy, The University of Texas at San Antonio, San Antonio, Texas 78249, United States*
Ivan K. Schuller − *Center for Advanced Nanoscience and Department of Physics, University of California, San Diego, La Jolla, California 92093, United States*

Complete contact information is available at: https://pubs.acs.org/10.1021/acsanm.0c00052

Notes

The authors declare no competing financial interest.

■ ACKNOWLEDGMENTS

This was a highly collaborative effort. The magnetic sample fabrication and characterization were supported by the U.S. Department of Energy's Office of Basic Energy Science, DMR, under Grant DE FG02 87ER-45332. The alumina shadow mask fabrication was supported by a collaborative NSF Grant DMR 1804414 and 1805585. R.M. acknowledges funding from Spanish Grant AEI-MINECO FIS2016-76058, UE FEDER "Una manera de hacer Europa", the European Unioń s Horizon 2020 research and innovation program under the Marie Sklodowska-Curie Grant Agreement No. 734801, and the Basque Government, PIBA 2018-11 and IT1162-19. A.N.F acknowledges research funding support from the Office of Undergraduate Research and the College of Science at the University of Texas at San Antonio.

■ REFERENCES

(1) Martin, J. I.; Nogues, J.; Liu, K.; Vicent, J. L.; Schuller, I. K. Ordered magnetic nanostructures: fabrication and properties. *J. Magn. Magn. Mater.* **2003**, *256* (1−3), 449−501.
(2) Nogues, J.; Sort, J.; Langlais, V.; Skumryev, V.; Surinach, S.; Munoz, J. S.; Baro, M. D. Exchange bias in nanostructures. *Phys. Rep.* **2005**, *422* (3), 65−117.
(3) Skomski, R. Nanomagnetics. *J. Phys.: Condens. Matter* **2003**, *15* (20), R841−R896.
(4) Navas, D.; Nam, C.; Velazquez, D.; Ross, C. A. Shape and strain-induced magnetization reorientation and magnetic anisotropy in thin film Ti/CoCrPt/Ti lines and rings. *Phys. Rev. B: Condens. Matter Mater. Phys.* **2010**, *81* (22), 224439.
(5) Maziewski, A.; Zablotskii, V.; Kisielewski, M. Geometry-driven out-of-plane magnetization states in nanostructures. *Phys. Rev. B: Condens. Matter Mater. Phys.* **2006**, *73* (13), 134415.
(6) Skumryev, V.; Stoyanov, S.; Zhang, Y.; Hadjipanayis, G.; Givord, D.; Nogues, J. Beating the superparamagnetic limit with exchange bias. *Nature* **2003**, *423* (6942), 850−3.
(7) Cowburn, R. P. Property variation with shape in magnetic nanoelements. *J. Phys. D: Appl. Phys.* **2000**, *33* (1), R1−R16.
(8) Klaui, M.; Vaz, C. A. F.; Lopez-Diaz, L.; Bland, J. A. C. Vortex formation in narrow ferromagnetic rings. *J. Phys.: Condens. Matter* **2003**, *15* (21), R985−R1024.
(9) Buchanan, K. S.; Roy, P. E.; Grimsditch, M.; Fradin, F. Y.; Guslienko, K. Y.; Bader, S. D.; Novosad, V. Soliton-pair dynamics in patterned ferromagnetic ellipses. *Nat. Phys.* **2005**, *1* (3), 172−176.
(10) Kim, D. H.; Rozhkova, E. A.; Ulasov, I. V.; Bader, S. D.; Rajh, T.; Lesniak, M. S.; Novosad, V. Biofunctionalized magnetic-vortex microdiscs for targeted cancer-cell destruction. *Nat. Mater.* **2010**, *9* (2), 165−71.
(11) Vogel, A.; Kamionka, T.; Martens, M.; Drews, A.; Chou, K. W.; Tyliszczak, T.; Stoll, H.; Van Waeyenberge, B.; Meier, G. Coupled vortex oscillations in spatially separated permalloy squares. *Phys. Rev. Lett.* **2011**, *106* (13), 137201.
(12) Morales, R.; Kovylina, M.; Schuller, I. K.; Labarta, A.; Batlle, X. Antiferromagnetic/ferromagnetic nanostructures for multidigit storage units. *Appl. Phys. Lett.* **2014**, *104* (3), 032401.
(13) Zhu, Q. Y.; Zheng, Q.; Liu, X. Y.; Wang, J. B.; Liu, Q. F. Phase locking of moving magnetic vortices in bridge-coupled nanodisks. *J. Appl. Phys.* **2015**, *117* (17), 173907.
(14) Mora, B.; Perez-Valle, A.; Redondo, C.; Boyano, M. D.; Morales, R. Cost-Effective Design of High-Magnetic Moment Nanostructures for Biotechnological Applications. *ACS Appl. Mater. Interfaces* **2018**, *10* (9), 8165−8172.
(15) Nogués, J.; Schuller, I. K. Exchange bias. *J. Magn. Magn. Mater.* **1999**, *192* (2), 203−232.
(16) Manna, P. K.; Yusuf, S. M. Two interface effects: Exchange bias and magnetic proximity. *Phys. Rep.* **2014**, *535* (2), 61−99.
(17) Luo, Z.; Dao, T. P.; Hrabec, A.; Vijayakumar, J.; Kleibert, A.; Baumgartner, M.; Kirk, E.; Cui, J.; Savchenko, T.; Krishnaswamy, G.; Heyderman, L. J.; Gambardella, P. Chirally coupled nanomagnets. *Science* **2019**, *363* (6434), 1435−1439.
(18) Meiklejohn, W. H.; Bean, C. P. New Magnetic Anisotropy. *Phys. Rev.* **1956**, *102* (5), 1413−1414.
(19) Morales, R.; Li, Z. P.; Olamit, J.; Liu, K.; Alameda, J. M.; Schuller, I. K. Role of the antiferromagnetic bulk spin structure on exchange bias. *Phys. Rev. Lett.* **2009**, *102* (9), 097201.
(20) Biternas, A. G.; Chantrell, R. W.; Nowak, U. Behavior of the antiferromagnetic layer during training in exchange-biased bilayers within the domain state model. *Phys. Rev. B: Condens. Matter Mater. Phys.* **2010**, *82* (13), 134426.
(21) Schuller, I. K.; Morales, R.; Batlle, X.; Nowak, U.; Guntherodt, G. Role of the antiferromagnetic bulk spins in exchange bias. *J. Magn. Magn. Mater.* **2016**, *416*, 2−9.
(22) Cortie, D. L.; Biternas, A. G.; Chantrell, R. W.; Wang, X. L.; Klose, F. Microscopic model for exchange bias from grain-boundary disorder in a ferromagnet/antiferromagnet thin film with a nanocrystalline microstructure. *Appl. Phys. Lett.* **2014**, *105* (3), 032402.
(23) Hsu, J. H.; Sun, A. C.; Sharma, P. Lateral grain size effect on exchange bias in polycrystalline NiFe/FeMn bilayer films. *Thin Solid Films* **2013**, *542*, 87−90.
(24) Kim, K. Y.; Choi, H. C.; Jo, S. Y.; You, C. Y. Enhancement of exchange bias field in top-pinned FeMn/Py bilayers with Ta/Cu hybrid underlayers. *J. Appl. Phys.* **2013**, *114* (7), 073908.
(25) Kohn, A.; Kovacs, A.; Fan, R.; McIntyre, G. J.; Ward, R. C.; Goff, J. P. The antiferromagnetic structures of $IrMn_3$ and their influence on exchange-bias. *Sci. Rep.* **2013**, *3*, 2412.
(26) Mlynczak, E.; Matlak, B.; Koziol-Rachwal, A.; Gurgul, J.; Spiridis, N.; Korecki, J. Fe/CoO(001) and Fe/CoO(111) bilayers: Effect of crystal orientation on the exchange bias. *Phys. Rev. B: Condens. Matter Mater. Phys.* **2013**, *88* (8), 085442.
(27) Saerbeck, T.; Zhu, H.; Lott, D.; Lee, H.; LeClair, P. R.; Mankey, G. J.; Stampfl, A. P. J.; Klose, F. Tailoring exchange bias through chemical order in epitaxial $FePt_3$ films. *J. Appl. Phys.* **2013**, *114* (1), 013901.
(28) van der Zaag, P. J.; Ijiri, Y.; Borchers, J. A.; Feiner, L. F.; Wolf, R. M.; Gaines, J. M.; Erwin, R. W.; Verheijen, M. A. Difference between blocking and Neel temperatures in the exchange biased Fe_3O_4/CoO system. *Phys. Rev. Lett.* **2000**, *84*, 6102−5.
(29) Sang, H.; Du, Y. W.; Chien, C. L. Exchange coupling in $Fe_{50}Mn_{50}/Ni_{81}Fe_{19}$ bilayer: Dependence on antiferromagnetic layer thickness. *J. Appl. Phys.* **1999**, *85* (8), 4931−4933.
(30) Mishra, S. K.; Radu, F.; Valencia, S.; Schmitz, D.; Schierle, E.; Durr, H. A.; Eberhardt, W. Dual behavior of antiferromagnetic uncompensated spins in NiFe/IrMn exchange biased bilayers. *Phys. Rev. B: Condens. Matter Mater. Phys.* **2010**, *81* (21), 212404.
(31) Morales, R.; Basaran, A. C.; Villegas, J. E.; Navas, D.; Soriano, N.; Mora, B.; Redondo, C.; Batlle, X.; Schuller, I. K. Exchange-bias phenomenon: the role of the ferromagnetic spin structure. *Phys. Rev. Lett.* **2015**, *114* (9), 097202.

(32) Zhang, W.; Krishnan, K. M. Epitaxial exchange-bias systems: From fundamentals to future spin-orbitronics. *Mater. Sci. Eng., R* **2016**, *105*, 1−20.
(33) Shi, H.; Lederman, D.; O'Donovan, K. V.; Borchers, J. A. Exchange bias and enhancement of the Néel temperature in thin NiF_2 films. *Phys. Rev. B: Condens. Matter Mater. Phys.* **2004**, *69* (21), 214416.
(34) Lang, X. Y.; Zheng, W. T.; Jiang, Q. Dependence of the blocking temperature in exchange biased ferromagnetic/antiferromagnetic bilayers on the thickness of the antiferromagnetic layer. *Nanotechnology* **2007**, *18* (15), 155701.
(35) Gomonay, H. V.; Loktev, V. M. Shape-induced phenomena in finite-size antiferromagnets. *Phys. Rev. B: Condens. Matter Mater. Phys.* **2007**, *75* (17), 174439.
(36) Li, Z. P.; Morales, R.; Schuller, I. K. Relevance of length scales in exchange biased submicron dots. *Appl. Phys. Lett.* **2009**, *94* (14), 142503.
(37) Perzanowski, M.; Krupinski, M.; Zarzycki, A.; Dziedzic, A.; Zabila, Y.; Marszalek, M. Exchange Bias in the $[CoO/Co/Pd]_{10}$ Antidot Large Area Arrays. *ACS Appl. Mater. Interfaces* **2017**, *9* (38), 33250−33256.
(38) Carrico, A. S.; Camley, R. E.; Stamps, R. L. Phase diagram of thin antiferromagnetic films in strong magnetic fields. *Phys. Rev. B: Condens. Matter Mater. Phys.* **1994**, *50* (18), 13453−13460.
(39) Baltz, V.; Sort, J.; Landis, S.; Rodmacq, B.; Dieny, B. Tailoring size effects on the exchange bias in ferromagnetic-antiferromagnetic < 100 nm nanostructures. *Phys. Rev. Lett.* **2005**, *94* (11), 117201.
(40) Laureti, S.; Suck, S. Y.; Haas, H.; Prestat, E.; Bourgeois, O.; Givord, D. Size dependence of exchange bias in Co/CoO nanostructures. *Phys. Rev. Lett.* **2012**, *108* (7), 077205.
(41) Liu, K.; Baker, S. M.; Tuominen, M.; Russell, T. P.; Schuller, I. K. Tailoring exchange bias with magnetic nanostructures. *Phys. Rev. B: Condens. Matter Mater. Phys.* **2001**, *63* (6), 060403.
(42) Malinowski, G.; Albrecht, M.; Guhr, I. L.; Coey, J. M. D.; van Dijken, S. Size-dependent scaling of perpendicular exchange bias in magnetic nanostructures. *Phys. Rev. B: Condens. Matter Mater. Phys.* **2007**, *75* (1), 012413.
(43) Menéndez, E.; Modarresi, H.; Petermann, C.; Nogués, J.; Domingo, N.; Liu, H.; Kirby, B. J.; Mohd, A. S.; Salhi, Z.; Babcock, E.; Mattauch, S.; Van Haesendonck, C.; Vantomme, A.; Temst, K. Lateral Magnetically Modulated Multilayers by Combining Ion Implantation and Lithography. *Small* **2017**, *13* (11), 1603465.
(44) Hibino, Y.; Hirai, T.; Hasegawa, K.; Koyama, T.; Chiba, D. Enhancement of the spin-orbit torque in a Pt/Co system with a naturally oxidized Co layer. *Appl. Phys. Lett.* **2017**, *111* (13), 132404.
(45) Wang, K.; Sanderink, J. G. M.; Bolhuis, T.; van der Wiel, W. G.; de Jong, M. P. Tunnelling anisotropic magnetoresistance due to antiferromagnetic CoO tunnel barriers. *Sci. Rep.* **2015**, *5* (1), 15498.
(46) Navarro-Senent, C.; Fornell, J.; Isarain-Chávez, E.; Quintana, A.; Menéndez, E.; Foerster, M.; Aballe, L.; Weschke, E.; Nogués, J.; Pellicer, E.; Sort, J. Large Magnetoelectric Effects in Electrodeposited Nanoporous Microdisks Driven by Effective Surface Charging and Magneto-Ionics. *ACS Appl. Mater. Interfaces* **2018**, *10* (51), 44897−44905.
(47) De Toro, J. A.; Marques, D. P.; Muniz, P.; Skumryev, V.; Sort, J.; Givord, D.; Nogues, J. High Temperature Magnetic Stabilization of Cobalt Nanoparticles by an Antiferromagnetic Proximity Effect. *Phys. Rev. Lett.* **2015**, *115* (5), 057201.
(48) Miltenyi, P.; Gierlings, M.; Keller, J.; Beschoten, B.; Guntherodt, G.; Nowak, U.; Usadel, K. D. Diluted antiferromagnets in exchange bias: proof of the domain state model. *Phys. Rev. Lett.* **2000**, *84* (18), 4224−7.
(49) Gredig, T.; Krivorotov, I. N.; Eames, P.; Dahlberg, E. D. Unidirectional coercivity enhancement in exchange-biased Co/CoO. *Appl. Phys. Lett.* **2002**, *81* (7), 1270−1272.
(50) Chen, S. W.; Lu, X.; Blackburn, E.; Lauter, V.; Ambaye, H.; Chan, K. T.; Fullerton, E. E.; Berkowitz, A. E.; Sinha, S. K. Nonswitchable magnetic moments in polycrystalline and (111)-epitaxial permalloy/CoO exchange-biased bilayers. *Phys. Rev. B: Condens. Matter Mater. Phys.* **2014**, *89* (9), 094419.
(51) Brems, S.; Buntinx, D.; Temst, K.; Van Haesendonck, C.; Radu, F.; Zabel, H. Reversing the training effect in exchange biased CoO/Co bilayers. *Phys. Rev. Lett.* **2005**, *95* (15), 157202.
(52) Roy, S.; Sanchez-Hanke, C.; Park, S.; Fitzsimmons, M. R.; Tang, Y. J.; Hong, J. I.; Smith, D. J.; Taylor, B. J.; Liu, X.; Maple, M. B.; Berkowitz, A. E.; Kao, C. C.; Sinha, S. K. Evidence of modified ferromagnetism at a buried Permalloy/CoO interface at room temperature. *Phys. Rev. B: Condens. Matter Mater. Phys.* **2007**, *75* (1), 014442.
(53) Chang, S. C.; Tsay, J. S.; Chang, C. H. T.; Yao, Y. D. Pinning of magnetic moments at the interfacial region of ultrathin CoO/Co bilayers grown on Ge(100). *Appl. Surf. Sci.* **2015**, *354*, 95−99.
(54) Matsukura, F.; Tokura, Y.; Ohno, H. Control of magnetism by electric fields. *Nat. Nanotechnol.* **2015**, *10* (3), 209−20.
(55) Girgis, E.; Portugal, R. D.; Loosvelt, H.; Van Bael, M. J.; Gordon, I.; Malfait, M.; Temst, K.; Van Haesendonck, C.; Leunissen, L. H.; Jonckheere, R. Enhanced asymmetric magnetization reversal in nanoscale Co/CoO arrays: competition between exchange bias and magnetostatic coupling. *Phys. Rev. Lett.* **2003**, *91* (18), 187202.
(56) Salazar-Alvarez, G.; Geshev, J.; Agramunt-Puig, S.; Navau, C.; Sanchez, A.; Sort, J.; Nogues, J. Tunable High-Field Magnetization in Strongly Exchange-Coupled Freestanding Co/CoO Core/Shell Coaxial Nanowires. *ACS Appl. Mater. Interfaces* **2016**, *8* (34), 22477−83.
(57) Menendez, E.; Modarresi, H.; Petermann, C.; Nogues, J.; Domingo, N.; Liu, H.; Kirby, B. J.; Mohd, A. S.; Salhi, Z.; Babcock, E.; Mattauch, S.; Van Haesendonck, C.; Vantomme, A.; Temst, K. Lateral Magnetically Modulated Multilayers by Combining Ion Implantation and Lithography. *Small* **2017**, *13* (11), 1603465.
(58) Guiliani, J.; Cadena, J.; Monton, C. Template-assisted electrodeposition of Ni and Ni/Au nanowires on planar and curved substrates. *Nanotechnology* **2018**, *29* (7), 075301.
(59) Zaraska, L.; Sulka, G. D.; Jaskula, M. Anodic alumina membranes with defined pore diameters and thicknesses obtained by adjusting the anodizing duration and pore opening/widening time. *J. Solid State Electrochem.* **2011**, *15* (11−12), 2427−2436.
(60) Valmianski, I.; Monton, C.; Schuller, I. K. Microscopy image segmentation tool: robust image data analysis. *Rev. Sci. Instrum.* **2014**, *85* (3), 033701.
(61) Suck, S. Y.; Neu, V.; Wolff, U.; Bahr, S.; Bourgeois, O.; Givord, D. Magnetic force microscopy analysis of magnetization reversal in exchange-biased Co/CoO nanostructure arrays. *Appl. Phys. Lett.* **2009**, *95* (16), 162503.
(62) Balcells, L.; Martinez, B.; Iglesias, O.; Garcia-Martin, J. M.; Cebollada, A.; Garcia-Martin, A.; Armelles, G.; Sepulveda, B.; Alaverdyan, Y. Exchange bias in laterally oxidized Au/Co/Au nanopillars. *Appl. Phys. Lett.* **2009**, *94* (6), 062502.
(63) Malozemoff, A. P. Random-field model of exchange anisotropy at rough ferromagnetic-antiferromagnetic interfaces. *Phys. Rev. B: Condens. Matter Mater. Phys.* **1987**, *35* (7), 3679−3682.
(64) Miguel, J.; Abrudan, R.; Bernien, M.; Piantek, M.; Tieg, C.; Kirschner, J.; Kuch, W. Magnetic domain coupling study in single-crystalline Fe/CoO bilayers. *J. Phys.: Condens. Matter* **2009**, *21* (18), 185004.
(65) Hussain, Z.; Reddy, V. R. Kerr microscopy study of thermal and athermal training effects in a Co/CoO exchange bias system. *J. Appl. Phys.* **2017**, *122* (10), 103903.
(66) Hussain, Z.; Reddy, V. R. Role of anti-ferromagnetic layer thickness in exchange bias: case study of Co/CoO with Kerr microscopy. *Mater. Res. Express* **2019**, *6* (6), 066109.
(67) Smith, N.; Cain, W. C. Micromagnetic model of an exchange coupled NiFe-TbCo bilayer. *J. Appl. Phys.* **1991**, *69* (4), 2471−2479.
(68) Roshchin, I. V.; Petracic, O.; Morales, R.; Li, Z. P.; Batlle, X.; Schuller, I. K. Lateral length scales in exchange bias. *Europhys. Lett.* **2005**, *71* (2), 297−303.
(69) Olamit, J.; Arenholz, E.; Li, Z.-P.; Petracic, O.; Roshchin, I. V.; Morales, R.; Batlle, X.; Schuller, I. K.; Liu, K. Loop bifurcation and

https://dx.doi.org/10.1021/acsanm.0c00052
ACS Appl. Nano Mater. XXXX, XXX, XXX−XXX

623 magnetization rotation in exchange-biased Ni/FeF_2. *Phys. Rev. B: Condens. Matter Mater. Phys.* **2005**, *72* (1), 012408.
625 (70) Petracic, O.; Li, Z. P.; Roshchin, I. V.; Viret, M.; Morales, R.; 626 Batlle, X.; Schuller, I. K. Bidomain state in exchange biased FeF_2/Ni. 627 *Appl. Phys. Lett.* **2005**, *87* (22), 222509.
628 (71) Gredig, T.; Krivorotov, I. N.; Dahlberg, E. D. Temperature 629 dependence of magnetization reversal and angular torque in Co/CoO. 630 *Phys. Rev. B: Condens. Matter Mater. Phys.* **2006**, *74* (9), 094431.
631 (72) Gruyters, M. Cobalt oxide/ferromagnet bilayers: Exchange 632 coupling and dominance of the antiferromagnet. *Europhys. Lett.* **2003**, 633 *64* (6), 803−809.

https://dx.doi.org/10.1021/acsanm.0c00052
ACS Appl. Nano Mater. XXXX, XXX, XXX−XXX